Invisibility on demand based on a generalized Hilbert transform

Zeki Hayran[1,*], Ramon Herrero[2], Muriel Botey[2], Hamza Kurt[1], and Kestutis Staliunas[2,3]

[1]*Department of Electrical and Electronics Engineering, TOBB University of Economics and Technology, Ankara 06560, Turkey*
[2]*Departament de Física, Universitat Politècnica de Catalunya (UPC), Colom 11, E-08222 Terrassa, Barcelona, Spain*
[3]*Institució Catalana de Recerca i Estudis Avançats (ICREA), Passeig Lluís Companys 23, E-08010, Barcelona, Spain*

We propose a feasible invisibility approach to suppress the scattering of waves from/to given directions and for particular frequencies, *i.e.* invisibility on demand. We derive a generalized Hilbert transform for a specific invisibility arrangement relating the two quadratures of the complex permittivity of an object. The scheme allows either designing objects to be invisible, or alternatively modifying the complex susceptibility of a given object to render invisibility. The theoretical proposal is further confirmed by finite-difference time-domain numerical calculations. Moreover, following an iterative chain of generalized Hilbert transforms, we propose the invisibility on demand with additional constraints, i.e. restricting the required modification of the complex refractive index within practical limits by avoiding gain areas. The proposed concept not only opens a new venue of real or complex valued index landscapes; but also bridges the gap between Hermitian and non-Hermitian optical systems by unifying these systems under one single generalized design theory.

Full invisibility, or cloaking, was proposed using transformation optics or, equivalently, conformal mapping [1,2]. The idea is elegant and fascinating; however, it can hardly cross the limits of science fiction, since the complexity of the required metamaterials severely limit practical realizations. Therefore, actual cloaking schemes generally scarify the perfect wavefront reconstruction or operate under a narrow bandwidth, as for instance in carpet cloaking [3-7], plasmonic cloaking [8,9], or mantle cloaking with thin patterned metasurfaces [10], metallic scatterer [11] or dielectric coating [12] based cloaking, among others [13,14].

A completely different approach to the concept of invisibility, referred as "unidirectional invisibility", relays on systems described by non-Hermitian Hamiltonians [15-17]. The concept is based on the property of an object to be invisible when probed by a wave from one side only. Such effect is accomplished by specific complex-modulated potentials (in optical terms: specific refraction index and gain/loss distributions), that allow suppressing the scattering of radiation from an object.

Unidirectional invisibility was first proposed for parity-time (PT) symmetric periodical systems (defined by symmetric index modulations accompanied by anti-symmetric gain/loss distributions), close to so-called PT-symmetry breaking point. Initially proposed for narrow frequency bands (due to the resonances of the periodic structure), and for particular incidence directions [18-20], the idea was extended to broad band radiation (both in frequency and in propagation direction) also by considering non-PT-symmetric potentials [21-25].

More recently, "unidirectional invisibility" has been related to the more general class of non-Hermitian potentials fulfilling the spatial Kramers-Kronig (KK) relations [26]. In the same way as the causality in time imposes KK relations in frequency, analogously, the KK theory may be directly extended to attain unidirectional invisibility in space. Yet temporal causality implies "invisibility of the future", so the response function $\chi(t)$, which is the kernel in the integral expression of the response of any physical system $A_{\mathrm{resp}}(t) = \int A_{\mathrm{sign}}(t - t_1)\chi(t)\mathrm{d}t_1$, must be zero for all $t > 0$. Such response function in time domain, $\chi(t)$, being $\chi(t) = 0$ for $t > 0$, determines the integral relations between the real and imaginary parts of its spectrum, $\chi_{\mathrm{im}}(\omega) = \frac{1}{\pi} P \int_{-\infty}^{\infty} \frac{\chi_{\mathrm{re}}(\omega_1)}{(\omega-\omega_1)} \mathrm{d}\omega_1$, and $\chi_{\mathrm{re}}(\omega) = \frac{-1}{\pi} P \int_{-\infty}^{\infty} \frac{\chi_{\mathrm{im}}(\omega_1)}{(\omega-\omega_1)} \mathrm{d}\omega_1$, where P means the Cauchy principle value of the integral. This KK relation (or more generally Hilbert transform) in frequency domain can be directly rewritten in space domain. The spatial invisibility requires that the scattering function fulfills $\chi(\mathbf{k}) = 0$ for all $\mathbf{k} = (k_x, k_y, k_z)$ with $k_x < 0$, i.e. it vanishes on the entire left half-space in wavevector domain. Throughout the letter, the invisibility on demand is formulated in two spatial dimensions (2D), and may be straightforwardly extended to 3D. Such a condition in the 2D **k**-space, (k_x, k_y), leads to similar KK relations in space domain: $\chi_{\mathrm{im}}(x, y) = \frac{1}{\pi} P \int_{-\infty}^{\infty} \frac{\chi_{\mathrm{re}}(x_1,y)}{(x-x_1)} \mathrm{d}x_1$, and $\chi_{\mathrm{re}}(x, y) = \frac{-1}{\pi} P \int_{-\infty}^{\infty} \frac{\chi_{\mathrm{im}}(x_1,y)}{(x-x_1)} \mathrm{d}x_1$. Therefore, the spatial KK relations are at the basis of unidirectional invisibility: all plane waves propagating from left to right $k_x > 0$, will not be back-scattered by such potentials, since they are uncoupled from the waves propagating to the left $k_x < 0$, as illustrated in Figs. 1(a) and 1(b). Following the spatial KK approach, a limited bidirectional invisibility has also been proposed, however restricted to small incident angles onto the interface (grazing incidence), by manipulating the reference point of the wavevectors cut-off [24]; bidirectional invisibility was also previously predicted in PT-symmetric systems for a given number of unit-cells [25].

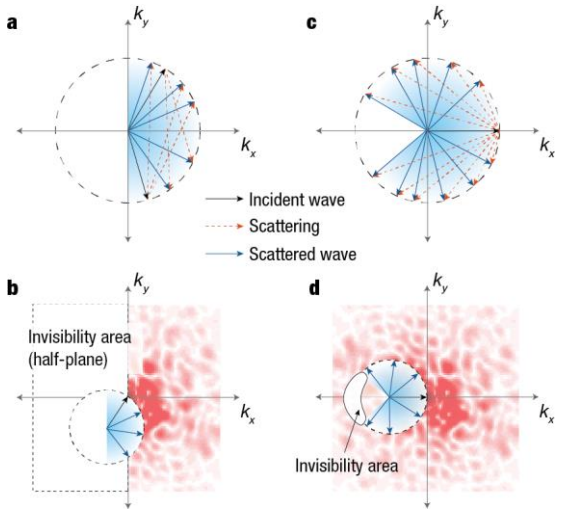

FIG. 1. (color online) Illustration of unidirectional invisibility and invisibility on demand. (a) In full unidirectional invisibility, in order to prevent left-reflection of every right-propagating wave, (b) all modulation components on the left half-plane, k_x<0, in $\mathbf{k}=(k_x,k_y)$ space, must be set to zero. (c) For invisibility on demand, to prevent back-scattering in a particular angular range (d) the modulation components to be set to zero are just the ones within a limited invisibility area in $\mathbf{k}=(k_x,k_y)$ space. In particular, the invisibility case (**c**) requires uncoupling the scattering of incident waves around $\mathbf{k}=(k_0,0)$ into back reflections, i.e. into waves in the vicinity of $\mathbf{k}=(-k_0,0)$; then, the invisibility function has to be centered at $\mathbf{k}=(-2k_0,0)$.

We propose here invisibility on demand: we derive an explicit integral relation, which may be regarded as a generalized Hilbert transform, associated with an arbitrary area of invisibility in **k**-space, see the schematic illustration on Figs. 1(c) and (d). In other words, we propose a procedure to modify the scattering from an object, being either a refractive index scatterer or a complex scatterer including index and gain/loss profiles, in such a way that the object becomes invisible for a range of frequencies and illumination/detection arrangement, depending on the required situation.

The main motivation for the invisibility on demand is facing invisibility under a realistic scope. First, generally full unidirectional invisibility may not be needed in many situations. Moreover, unidirectional invisibility requires a rather severe modification of the potential: if the refraction index - proportional to real part of susceptibility function of the potential, $\chi_{\mathrm{re}}(x,y)$ - is modulated with a specific amplitude, then the required profile of the imaginary part of susceptibility $\chi_{\mathrm{im}}(x,y)$ to render the object invisible, is of the same order of magnitude, as follows directly from the spatial KK relations. In our case, for invisibility on demand, the modification of the complex optical potential, depends upon the area of invisibility in **k**-space. Thus, the proposed scheme of invisibility on demand, working solely for special angular ranges and frequencies is substantially more feasible, as shown in details below. Besides, for unidirectional invisibility as based on spatial KK relations the imaginary part of susceptibility decays weakly, as $1/|x|$; which may result inadequate for applications since, as a consequence, the norm of the total gain/loss modification function diverges logarithmically. We show that invisibility under demand, in particular for smooth invisibility boundaries, leads to more convenient asymptotic behaviors (an exponential decay in space, results in a finite norm).

In the letter, we first derive the generalized Hilbert transform, for an arbitrary area of invisibility in wavevector domain. Then, we provide a series of numerical finite-difference-time-domain (FDTD) simulations of different cases to prove the idea and illustrate its performance. Finally, we describe an iterative procedure to generate the complex potentials for invisibility on demand with additional restrictions, for instance avoiding the areas of gain or negative index materials.

Generalized Hilbert transform.—Let us consider scattering from a local modulation of the optical potential characterized by the electric permittivity profile $\chi_{\mathrm{re}}(x,y)=\chi_{\mathrm{background}}+a(x,y)$. (Local modulation means $a(x,y)\to 0$, for $(x,y)\to\infty$.) The first order scattering form factor $a(k_x,k_y)$ is simply the Fourier transform of $a(x,y)$: $a(k_x,k_y)=\frac{1}{2\pi}\int a(x,y)\exp(\mathrm{i}k_x x+\mathrm{i}k_y y)\mathrm{d}x\mathrm{d}y$ (for weak potentials, in the so-called Born approximation, secondary scattering can be neglected). Plane waves with carrier wave-vector $\mathbf{k}_0$ are scattered by each wavenumber component **k**, of the modulation of the potential, into $\mathbf{k}_1=\mathbf{k}+\mathbf{k}_0$. Therefore, preventing scattering for a given angular range and in a restricted frequency range, requires imposing that a specific area in **k**-space leads to no scattering, see Fig. 1(d) for illustration. Let us define the invisibility function $\theta(k_x,k_y)$ in such a way that $\theta(k_x,k_y)=1$ in the given area of invisibility, being $\theta(k_x,k_y)=0$ elsewhere. Next, we construct a new scattering function of the object as: $a_1(k_x,k_y)=a(k_x,k_y)-a(k_x,k_y)\theta(k_x,k_y)$, which only eliminates the scattering from the particular invisibility area in **k**-space. In spatial domain, this corresponds to the modification of the profile of the (complex) susceptibility by a generalized Hilbert-like transform: $a_1(x,y)=a(x,y)-\frac{1}{2\pi}\iint a(x_1,y_1)\theta(x-x_1,y-y_1)\mathrm{d}x_1\mathrm{d}y_1$, since the multiplication of functions in wavenumber domain results in convolution in space. Then, it merely remains to calculate the kernel of the convolution, as the inverse Fourier transform of the invisibility area, $\theta(k_x,k_y)$, and to compute the above convolution. This results in what may be regarded as a generalized Hilbert transform. In particular, the elimination of scattering from the entire left half-plane, i.e. $\theta(k_x,k_y)=0$ for all $k_x<0$, results in $\theta(x,y)=\frac{-\mathrm{i}}{\sqrt{2\pi}x}$, and the corresponding convolution leads to the conventional KK or Hilbert transform in space. We thus generalize the Hilbert transform for arbitrary area of invisibility, which results in a different kernel.

Only specific shapes of the invisibility area in **k**-space allow analytical expressions for the kernel of the convolution $\theta(x,y)$. For instance, circular or elliptical

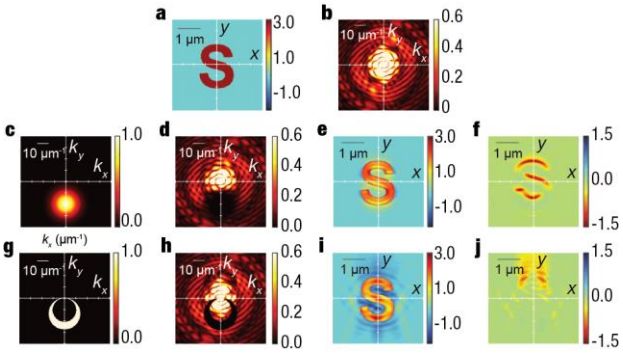

FIG. 2. (color online) Invisibility on demand procedure workflow in spatial and wavevector domain. Top: Initial object; (a) electric susceptibility and the (b) scattering potential. Center: Invisibility on demand by a Gaussian invisibility area, in the form of $\exp(-(k_x+2k_0)^2/(2\sigma_x^2)- (k_y+2k_0)^2/(2\sigma_y^2))$ centered at $-2*k_0=(k_x, k_y)=(0, 20)\mu m^{-1}$ with standard deviations of $\sigma_x=7.0\mu m^{-1}$ and $\sigma_y=7.0\mu m^{-1}$ in the k_x- and k_y- directions, respectively, in (c) kernel in **k**-space; (d) modified scattering potential; (e) real part and the (f) imaginary part of the of the susceptibility profile after 14 iterations. Bottom: Invisibility by an eclipse-shaped invisibility area; (g) invisibility area in **k**-space, (h) modified scattering potential; (i) real part and the (j) imaginary part of the of the susceptibility profile after 14 iterations.

invisibility areas result in Bessel functions in direct space (x, y) while square or rectangular areas of invisibility lead to sinc-shaped kernel functions. Some of such analytical cases are presented in the Appendix A. Especially interesting is the case of a ring-shaped invisibility, or a "partial-sun-eclipse" invisibility area, since it allows full unidirectional invisibility from a monochromatic plane probe wave. These two latter cases also allow analytical kernels, as derived in Appendix A.

Invisibility on demand may also be realized for smooth invisibility functions. For instance, if the considered invisibility function has Gaussian profile centered around some $-2\mathbf{k}_0$ point:$\theta(k_x, k_y) = exp(-(\mathbf{k} + 2\mathbf{k}_0)^2/\Delta k^2)$, then its inverse Fourier transform is also Gaussian, and leads to a convenient convolution kernel $\theta(x, y)$, with rapidly decreasing asymptotics.

As an example of a possible realization of invisibility on demand, we consider an "S" shaped object (see Figs. 2(a) and 2(b)) to be rendered invisible with respect to a circular invisibility area shown in Fig. 2(c). The modified object to be invisible under reflections (Figs. 2(e) and 2(f)) is simply calculated as the product of the object and the kernel spectra (Fig. 2(d)). The above described method can be performed with respect to any invisibility area in wavenumber domain, and any object. Another intriguing kernel type is the "solar eclipse" shaped invisibility area (see Figs. 2(g-j)), which yields elimination of reflection in a broad angular range.

Besides, we may apply an iterative approach that allows regularizing the complex scattering function with additional constrains, for instance excluding gain or negative index materials, yet allowing losses. In principle, the proposed invisibility scheme would typically lead to media with optical gain, and technical inconveniences might arise either for the fabrication of actual systems (within the conventional nanophotonics). Therefore, to avoid such difficulties, we apply a chain of Hilbert transforms where, at each iteration, negative imaginary parts of the complex susceptibility are completely eliminated by setting gain to zero. This operation is iteratively performed until the negative imaginary part is sufficiently reduced (its convergence depending on the initial refractive index, the size and shape of the invisibility hole). The analytical analysis of such an iterative approach is given in Appendix B.

The invisible object in **k**-space of Fig. 2(d) exhibits a shadowed region as compared to visible object, shown in Figs. 2(a) and 2(b) in direct and reciprocal space, respectively. It is interesting to remark that kernels with smooth profiles in **k**-space, introduce relatively small gain profiles in the modified object. On the contrary, stepwise profiles generate objects with symmetric gain and loss areas that, which however, can be easily converted into only loss areas using the iteration process described above.

To numerically verify the "invisibility on demand" proposal, we performed a series of numerical simulations based on the FDTD method [27]. For brevity, we present here the simulations only for transverse magnetic (TM) polarization (electric field perpendicular to the plane), however the procedure holds also for transverse electric (TE) polarization. Figures 3(a) and 3(b) and 3c show the steady state electric field distribution for different excitation angles before applying the invisibility procedure. Similarly, Figs. 3(d-f) and 3(g-i) depict the field distributions after applying the invisibility procedure for the Gaussian function and eclipse cases, respectively; exactly for the same illumination. It is clear that invisibility is achieved, when comparing the scattering of the object/modified object when illuminated by a probe source at different positions. Whereas scattered waves strongly interfere with incident light, a spatial region of uniform field distribution is a clear sign of invisibility. Moreover in Fig. 3(d), a partial standing wave effect outside the invisibility angular range can be observed. This is in particular due to the fact the scattered wavevectors outside the angular range do not lie inside the filtered wavevector region. On the other hand in Fig. 3(e), when all the scatterings lie inside the angular range, no standing wave is observed. Furthermore, to reveal the limits of the invisibility region in terms of both the operational wavelength and excitation angle, angle resolved reflection spectra calculations were performed. Figures 3(g) and 3(h) show the cases for which the invisibility is not-activated (R1) and activated (R2), respectively. By comparing Figs. 3(g) and 3(h), it can be inferred that by applying the invisibility on demand, a strong anti-reflection behavior can be achieved for a specific angle and frequency range. One fact to note is that the overall reflection decreases for nearly all excitation angles after applying the proposed procedure, however the decrease is substantially larger in the designed anti-reflection region. We attribute this fact to the increase of absorption losses. The ratio between R1 and R2, provided in Fig. 3(i) clearly reveals that the reduction of the

reflection is indeed significantly larger within the desired angle ranges and wavelengths. One important observation from Figs. 3(h) and 3(i) is that the deduced frequency range where the reflectivity decreases is lower than the designed frequency interval. This is in virtue of the fact that the Kramers-Kronig relations in the temporal domain imposes additional constraints to the frequency dispersion of the designed profiles, such that the profiles do not behave as invisible potentials anymore outside a certain frequency range. Here, we also note the fact that although our design approach is based on the Born approximation, these results suggest than an object with an initial refractive index as high as 2.0 can be rendered invisible since the removal of the first-order scattered waves can also lead to the elimination of the higher order scatterings [26], indicating that the concept is not inherently limited by the Born-approximation (which typically requires a very low index contrast on the order of 0.001), see Appendix C. Numerical simulations confirm the robustness of the invisibility on demand proposed scheme also at higher refractive indices. The method is flexible and feasible. It can be applied to arbitrarily-shaped objects, see Appendix D; and by purely real scattering functions, as demonstrated in Appendix E. Interestingly, invisibility areas with even functions in **k**-space directly result, following the Hilbert transform procedure, in purely real scattering functions; in this case, moreover, no iterative procedure is required.

To conclude, we propose a generalized Hilbert transform relating the two quadratures of the complex susceptibility of an object, to provide invisibility with respect to particular illumination/detection arrangements, and for particular frequencies corresponding to arbitrary demands. The invisibility on demand scheme allows either designing objects to be invisible, or alternatively modifying the complex susceptibility of a given object to render invisibility. The scheme succeeds not only in rendering invisible a passively scattering object, characterized by a real susceptibility (with neither gain nor losses), but also for arbitrary complex-valued scattering functions $\chi_{\mathrm{re}}(x,y)$. The procedure turns out to be more flexible than the spatial KK transform, while also allowing to form objects with topologically complex shapes at higher dimensions as opposed to previous demonstrations [28,29]. Furthermore, while a recent work has studied the reflectionless property for deformed analytic profiles [30], the proposed method provides a much a more flexible way to create invisible profiles that are extremely complex in shape and that are invisible only for designated angular ranges and frequencies. Moreover, following an iterative chain of generalized Hilbert transforms, we propose the invisibility on demand with additional constraints, *i.e.* restricting the required modification of the complex refractive index within practical limits by avoiding gain areas. Such lossy profiles can be experimentally realized at optical frequencies by locally tuning the material absorption [31-33] or by tailoring the out-of-plane radiation losses [34].

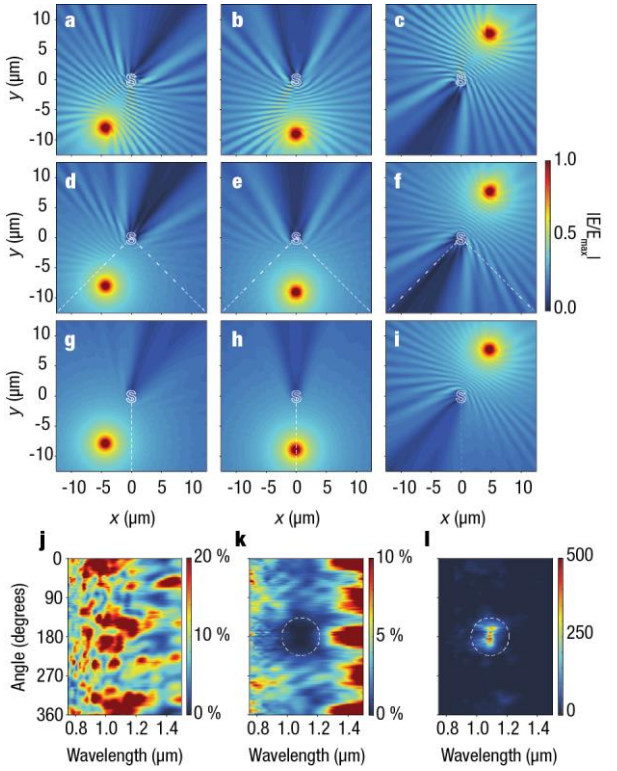

FIG. 3. (color online) Invisibility on demand performance. FDTD simulations for the "S" shaped object (given in Fig. 2(a)), probed by a monochromatic (λ_0=1.1μm) point source at different angular positions, from left to right: 208°, 180° and 32° (with respect to a vertical axis, in clockwise direction), when: invisibility is (a),(b),(c) not-activated and (d-i) activated with the same invisibility function as in Fig. 2(c) (for (d-f)) and Fig. 2(g) (for (g-i)) after 14 iterations. The scatterer is outlined by white solid lines. The white dashed lines show the angular range of invisibility on demand. For a full angular analysis, see Supplementary Movie 1. Angle-wavelength scattering spectra obtained with a plane wave source, for (j) invisibility not-activated and (k) activated. (l) Relative scattering (ratio between scattering spectra for inactivated and activated invisibility) in angle-wavelength domain.

While being feasible in optics, gain materials may result inconvenient, and they remain very challenging for other kind of waves, for instance in acoustics. The procedure is theoretically presented and supported by FDTD numerical simulations of arbitrary-shaped objects.

We present here the basic idea of invisibility on demand, leaving the different aspects of the concept in the appendix: analytically solvable invisibility functions; also special cases leading to broad angle invisibility cloaking, and other more complex cases. The proposed scheme primarily discussed in optics, in principle is working in other fields of wave dynamics.

ACKNOWLEDGEMENTS

Authors acknowledge financial support of NATO SPS research grant No: 985048, support from Spanish Ministerio de Ciencia e Innovación, and European Union FEDER through project FIS2015-65998-C2-1-P, and partial support of the Turkish Academy of Sciences.

APPENDIX A: ANALYTICAL KERNELS

Some invisibility functions, or different shapes of the invisibility area, allow obtaining analytical expressions for the kernels of the generalized Hilbert transform. Here we list some of them.

The kernel of an elliptical (rectangular) invisibility area, centered around the wavevector of the probe wave is expressed in Bessel (Sinc) functions:

$$\theta(k_x,k_y)=\mathrm{Disc}\left(\sqrt{\left(\frac{k_x+2k_0}{w_x}\right)^2+\left(\frac{k_y}{w_y}\right)^2}\right)\rightarrow\theta(x,y)=w_xw_y\,e^{\mathrm{i}\frac{2k_0x}{w_x}}\frac{J_1\left(\sqrt{w_x^2x^2+w_y^2y^2}\right)}{\sqrt{w_x^2x^2+w_y^2y^2}} \tag{A1}$$

$$\left(\theta(k_x,k_y)=\mathrm{Rect}\left(\frac{k_x+2k_0}{w_x}\right)\mathrm{Rect}\left(\frac{k_y}{w_y}\right)\rightarrow\theta(x,y)=w_xw_y\,e^{\mathrm{i}\frac{2k_0x}{w_x}}\,\mathrm{Sinc}(w_xx)\mathrm{Sinc}(w_yy)\right) \tag{A2}$$

These cases are presented in Fig. 4(a-c) and (d-f).

The invisibility area in form of a ring corresponding to all possible scattered wavevectors of fixed frequency, is of a special interest, since it allows full invisibility with respect to an incident monochromatic plane wave, in a given direction. The difference of two *Disc* functions with different radii $k_0(1+w)$ and $k_0(1-w)$, results in a ring with a width, $2wk_0$:

$$\theta(k_x,k_y)=\mathrm{Disc}\left(\sqrt{1-w}\sqrt{\left(\frac{k_x}{k_0}+1\right)^2+\left(\frac{k_y}{k_0}\right)^2}\right)-\mathrm{Disc}\left(\sqrt{1+w}\sqrt{\left(\frac{k_x}{k_0}+1\right)^2+\left(\frac{k_y}{k_0}\right)^2}\right)$$

$$\rightarrow\theta(x,y)=\frac{k_0^2}{1-w}e^{\mathrm{i}x\sqrt{1-w}}\frac{J_1\left(\sqrt{\frac{k_0^2}{1-w}(x^2+y^2)}\right)}{\sqrt{\frac{k_0^2}{1-w}(x^2+y^2)}}-\frac{k_0^2}{1+w}e^{\mathrm{i}x\sqrt{1+w}}\frac{J_1\left(\sqrt{\frac{k_0^2}{1+w}(x^2+y^2)}\right)}{\sqrt{\frac{k_0^2}{1+w}(x^2+y^2)}} \tag{A3}$$

As it is represented in Fig. 4(g-i).

Another interesting case is the "solar eclipse" shaped invisibility area given by the difference of two *Disc* functions with different radii touching at the origin $\mathbf{k}=0$, in **k**-space. This case allows covering all possible scattered wavevectors, keeping the incident monochromatic plane wave unaffected, obtaining the unidirectional cloaking effect. The width of the invisible area changes with the scattering angle, and becomes maximum at normal reflection. The analytical expression of this invisibility areas and corresponding kernel are:

$$\theta(k_x,k_y)=\mathrm{Disc}\left(\sqrt{\left(\frac{k_x}{k_0(1+w)}+1\right)^2+\left(\frac{k_y}{k_0(1+w)}\right)^2}\right)-\mathrm{Disc}\left(\sqrt{\left(\frac{k_x}{k_0(1-w)}+1\right)^2+\left(\frac{k_y}{k_0(1-w)}\right)^2}\right)$$

$$\rightarrow\theta(x,y)=k_0e^{\mathrm{i}x}\frac{(1+w)J_1\left(\sqrt{k_0(1+w)(x^2+y^2)}\right)-(1-w)J_1\left(\sqrt{k_0(1-w)(x^2+y^2)}\right)}{\sqrt{(x^2+y^2)}} \tag{A4}$$

Note that these last two cases, Figs. 4(g-i) and (j-l), lead to kernels which are weaker in amplitude, but more delocalized in space.

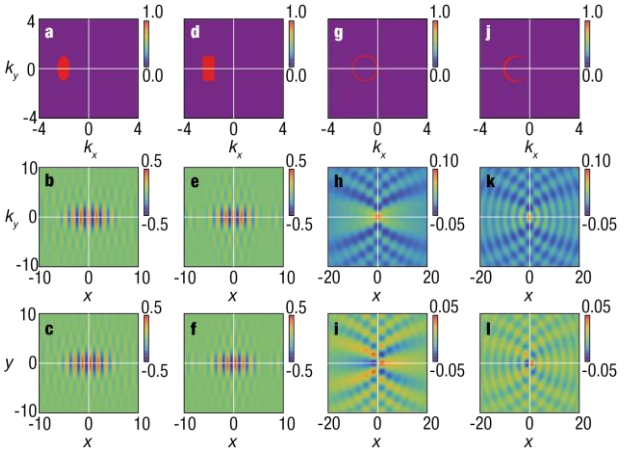

FIG. 4. Invisibility areas in Fourier space and corresponding kernels. Invisibility areas with: (a) elliptical shape (first column), (d) rectangular shape (second column) both with widths w_x=0.5k_0 and w_y=1.0k_0 —where k_0 is the input wavenumber of light— [which corresponds to 30º]; (g) complete circle shape (third column) and (j) "solar eclipse" shaped (fourth column) for these last two w=0.1λ_0. Corresponding associated kernels of the generalized Hilbert transform, (b),(e),(h),(k) real parts and (c),(f),(i),(l) imaginary parts.

APPENDIX B: ANALYTICAL CALCULATION OF INVISIBILITY ON DEMAND AND ITERATIVE PROCEDURE

This provides the calculation of the invisibility on demand procedure for a simple 1D or 2D Gaussian object (with either real or/and imaginary parts of the susceptibility) with a Gaussian invisibility function. In this case the analytical expressions are derived, which allow estimating the parameters of the system. In particular, it provides an estimation on the strength of the required modification of the potential to obtain invisibility on demand.

First, we consider a 1D Gaussian object of width x_0:

$$a(x)=a_0\exp(-x^2/x_0^2) \tag{A5}$$

with corresponding spectrum (Fourier transform),

$$a(k)=\frac{1}{\sqrt{2\pi}}\int a(x)\exp(-\mathrm{i}kx)\mathrm{d}x=\frac{x_0a_0}{\sqrt{2}}\exp(-k^2x_0^2/4) \tag{S6}$$

and we consider a Gaussian invisibility function:

$$\theta(k)=\exp(-(k+2k_0)^2/k_{\mathrm{inv}}^2) \tag{A7}$$

with halfwidth k_{inv}; being $k_0=\omega/c$ the wavevector of the object illumination (the invisibility function must be centered at around $-2k_0$ in order to prevent scattering from wavevector k_0 to $-k_0$).

The kernel of the generalized Hilbert transform is:

$$\theta(x)=\frac{1}{\sqrt{2\pi}}\int\theta(k)\exp(\mathrm{i}kx)\mathrm{d}x=\frac{\sqrt{2}}{x_{\mathrm{inv}}}\exp(-2\mathrm{i}k_0x-x^2/x_{\mathrm{inv}}^2). \tag{A8}$$

Here $x_{\mathrm{inv}}^2=4/k_{\mathrm{inv}}^2$.

According to the procedure described in the main article, the modification of the object is the corresponding convolution of the object susceptibility profile with the invisibility function. The calculation of such convolution in **k**-space results in:

$$a_1(x) = a(x) - \frac{1}{\sqrt{2\pi}} \int a(k)\theta(k)\exp(\mathrm{i}kx)\mathrm{d}k \quad \text{(A9)}$$

Inserting the Gaussian functions, and after some algebra, it follows that:

$$a_1(x) = a(x) - \frac{a_0 x_0}{x_1} \exp\left(-\mathrm{i}k_{c,1}x - \frac{x^2}{x_1^2} - \frac{x_0^2 x_{\mathrm{inv}}^2 k_0^2}{x_1^2}\right) \quad \text{(A10)}$$

The modification of the object results to be again a Gaussian function, centered at:

$$k_{c,1} = \frac{-2k_0 x_{\mathrm{inv}}^2}{x_1^2} \quad \text{(A11)}$$

in wavenumber domain, its width and amplitude being:

$$x_1^2 = x_0^2 + x_{\mathrm{inv}}^2; \qquad \frac{a_0 x_0}{x_1} exp\left(-\frac{x_0^2 x_{\mathrm{inv}}^2 k_0^2}{x_1^2}\right) \quad \text{(A12)}$$

Note that the modification of the object is a Gaussian function contains the oscillatory multiplier: $\exp(-\mathrm{i}k_{c,1}x)$. This indicates that the invisibility on demand introduces a modulation on the real and imaginary parts of susceptibility.

The relative norm of the correction (with respect to the norm of the initial object) is:

$$\exp\left(-\frac{x_0^2 x_{\mathrm{inv}}^2 k_0^2}{x_1^2}\right) \quad \text{(A13)}$$

which exponentially decreases with the decreasing area of invisibility in k-space.

The derived expression is valid for either an object with a Gaussian shape entailing only losses (being a_0 a real number) as well as for a Gaussian index profile (being a_0 imaginary), or for both simultaneously, i.e. for a complex index Gaussian profile.

In the limit of small invisibility area in **k**-space, $x_{\mathrm{inv}}^2 \gg x_0^2$, therefore assuming $x_1^2 \approx x_{\mathrm{inv}}^2$, the normalized correction function is:

$$\frac{\Delta a(x)}{a_0} \approx \frac{x_0}{x_{\mathrm{inv}}} exp\left(-2\mathrm{i}k_0 x - \frac{x^2}{x_{\mathrm{inv}}^2} - x_0^2 k_0^2\right) \quad \text{(A14)}$$

i.e. it is weak in amplitude, but broad in space; also, the modulation is centered at wavenumber $-k_{c,1} \approx -2\mathrm{i}k_0$. In the opposite limit, of a broad invisibility area in **k**-space, $x_{\mathrm{inv}}^2 \ll x_0^2$, and $x_1^2 \approx x_0^2$, leads to the correction function:

$$\frac{\Delta a(x)}{a_0} \approx \exp\left(-\mathrm{i}k_c x - \frac{x^2}{x_0^2} - x_{\mathrm{inv}}^2 k_0^2\right) \quad \text{(A15a)}$$

$$k_{c,1} = \frac{-2k_0 x_{\mathrm{inv}}^2}{x_0^2} \quad \text{(A15b)}$$

which is strong in amplitude (on the same order as the object itself), but narrow in space (nearly of the same width as the object); the modulation is centered at wavenumber $-k_{c,1} \approx 0$. However, in all cases the amplitude of the correction term is always smaller than the amplitude as the object itself.

As the correction of the scattering object (a_0 is real-valued) contains gain and loss (due to oscillatory factor $exp(-\mathrm{i}k_{c,1}x)$ in (S10), perhaps the simplest way to regularize the object (to remove the gain areas from a modified object in (S10) is to add the corresponding loss profile:

$$a_1(x) = a(x) - \frac{a_0 x_0}{x_1} \exp\left(-\mathrm{i}k_c x - \frac{x^2}{x_1^2} - \frac{x_0^2 x_{\mathrm{inv}}^2 k_0^2}{x_1^2}\right) + \mathrm{i}\frac{a_0 x_0}{x_1} \exp\left(-\frac{x^2}{x_1^2} - \frac{x_0^2 x_{\mathrm{inv}}^2 k_0^2}{x_1^2}\right) \quad \text{(A16)}$$

Such added loss profile will result in a weak scattering into invisibility domain (will spoil the invisibility achieved by (S10). This, however, can be removed again by using the same generalized Hilbert transform acting on (S16) rendering the object invisible again, by the next correction order:

$$\Delta a_1(x) = -\frac{a_0 x_0^2}{x_1 x_2} \exp\left(-\mathrm{i}k_{c,2}x - \frac{x^2}{x_2^2} - \frac{x_0^2 x_{\mathrm{inv}}^2 k_0^2}{x_2^2}\right) \quad \text{(A17)}$$

with the parameters (half-width, and center wavenumber):

$$x_2^2 = x_0^2 + 2x_{\mathrm{inv}}^2; \qquad k_{c,2} = \frac{-2k_0 x_{\mathrm{inv}}^2}{x_2^2} \quad \text{(A18)}$$

The procedure can be repeated, leading to a converging series. The convergence is assured since for each $x_n^2 = x_0^2 + nx_{\mathrm{inv}}^2$; $x_n^2 > x_0^2$, and $exp(-x_0^2 x_{\mathrm{inv}}^2 k_0^2/x_2^2)$<1. This proves that the invisibility on demand can always be obtained without gain for a Gaussian-shaped object, with a Gaussian invisibility function. This also hints how to construct and invisible on demand object without gain for arbitrary shaped object, and with an arbitrary invisibility function, however it does not provide a rigid proof.

The 1D Gaussian case can be directly extended to 2D, for elliptic areas of invisibility:

$$a(x,y) = a_0 \exp(-x^2/x_0^2 - y^2/y_0^2) \quad \text{(A19)}$$

$$\theta(k_x.k_y) = \exp\left(-(k_x + 2k_0)^2/k_{x,\mathrm{inv}}^2 - k_y^2/k_{y,\mathrm{inv}}^2\right) \quad \text{(A20)}$$

Inserting the Gaussian functions, and after some algebra, it follows that:

$$a_1(x,y) = a(x,y) - \frac{a_0 x_0 y_0}{x_1 y_1} exp\left(-\mathrm{i}k_{c,1}x - \frac{x^2}{x_1^2} - \frac{y^2}{y_1^2} - \frac{x_0^2 x_{\mathrm{inv}}^2 k_0^2}{x_1^2}\right) \quad \text{(A21)}$$

The procedure of regularization of (S21) is analogous to that in 1D case.

APPENDIX C: SOLAR ECLIPSE INVISIBILITY AREA

Next, we show how higher-order scattered waves may be efficiently suppressed by carefully designing the kernel, as for instance for the "solar eclipse" shaped invisibility region. To illustrate this, it is sufficient to inspect the *n*th term in the scattering series:

$$e_{\mathrm{s}}^{(n)}(k) = \frac{-k_0^2 G(k)}{2\pi} \int a(k-k')\tilde{e}_{\mathrm{s}}^{(n-1)}(k')\mathrm{d}k' \quad \text{(A22)}$$

where $e_{\mathrm{s}}^{(n)}$ is the nth-order scattered electric field, k_0 is the free space wavevector, $G(k) = (k_0^2 - k^2)^{-1}$ is the Fourier spectrum of retarded Green function, $a(k)$ and $\tilde{e}_{\mathrm{s}}(k)$ are the Fourier transforms of the complex potential and the scattered field, respectively. It can be directly seen from this equation that when $e_{\mathrm{s}}^{(1)}$ (first-order Born approximation) is completely suppressed, then every successive order will be also zero,

regardless of the value of other terms. Another way to understand this is to think that the eclipse actually eliminates all primary scattered propagating waves with respect to a particular plane wave of incidence. The secondary scattering, which is the dominating part of the second Born approximation then disappear as well, since the primarily scattered propagating waves are absent.

To illustrate this full invisibility, we employ the same "S" shaped object as in the above analyses and modify its complex susceptibility with a "solar eclipse" shaped kernel given in Fig. 2(g) (in the main article).

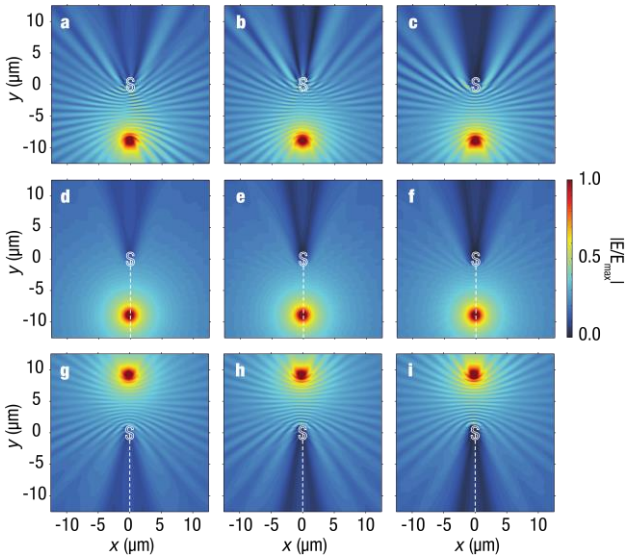

FIG. 5. Numerical results for the case of a "solar eclipse" shaped kernel with high refractive index contrasts. (a-i), FDTD simulations of waves coming from point sources at different positions towards the scatterer with an initial refractive index of (a,d,g) 2.0, (b,e,h) 3.0 and (c,f,i) 4.0. The upper row corresponds to the cases where the invisibility is not activated, the middle row corresponds to invisibility activated cases, and the lower row corresponds to cases where the invisibility is activated but where the source is located outside the invisibility range. The white dashed lines denote the incident angle where invisibility is activated. The operational wavelength is equal to 1.0μm.

Fig. 5(a-i) depicts the corresponding spatial field distributions under point source excitation for high initial refractive index contrasts of 2.0, 3.0 and 4.0. As it follows from these figures, scattering is almost fully suppressed in all directions and almost vanishes even for high index contrasts, as expected.

APPENDIX D: INVISIBILITY ON DEMAND PROCEDURE APPLIED ON COMPLEX SHAPED OBJECTS

To evidence that the proposed procedure holds also for complex shaped objects, we applied the invisibility on demand procedure for an "Einstein face" shaped object (with initial susceptibility of 2.3, see Fig. 6), and considering a Gaussian kernel placed at (k_x, k_y)=(0, -20.0)μm^{-1} and a standard deviation of 7.0μm^{-1} in both the k_x and k_y directions.

The FDTD simulations before and after applying the invisibility procedure are given in Fig. 7 at the operational wavelength of 1.10μm. It can be inferred from the figure that within the targeted angle range (delimited with white dashed lines) reflections are significantly suppressed, as the interference patterns between the probe source and reflections from the object are strongly suppressed.

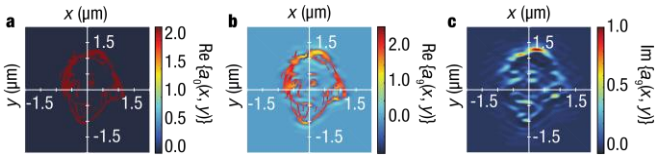

FIG. 6. Invisibility on demand procedure applied on a complex shaped object. (a-c) Complex susceptibility profiles of an "Einstein face" shaped object modified with a Gaussian invisibility area located at (k_x, k_y)=(0, -20.0)μm^{-1} with a standard deviation of 7.0μm^{-1} in both the k_x and k_y directions. (a) The real part of the initial object and the (b) real and (c) imaginary parts of the modified complex susceptibility after 9 iterations.

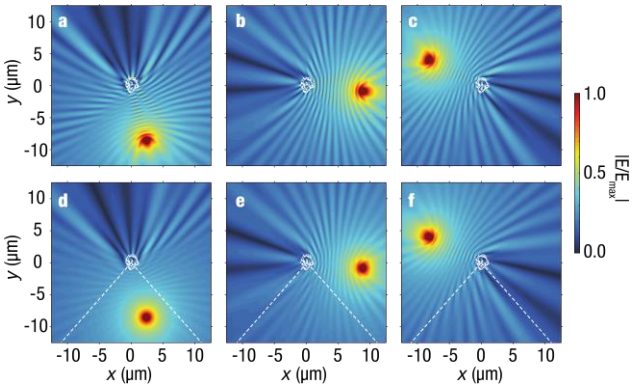

FIG. 7. Numerical results of a complex shaped scatterer. (a-f) FDTD simulations of waves coming from point sources at different positions. Scattering object is an "Einstein face" shaped object given in Fig. 6. The upper and lower rows correspond to cases where the invisibility is not-activated and activated, respectively. The white dashed lines denote the angle range where invisibility is activated. For a full angular analysis, see Supplementary Movie 2.

APPENDIX E: ALL-DIELECTRIC INVISIBLE OBJECTS

One interesting property of the proposed approach is that for symmetrically placed invisibility areas (that is to say for bidirectional invisibility at a specific angle and frequency range), the need for a gain loss modulation is completely eliminated (since the Fourier transform of an even function is purely real).

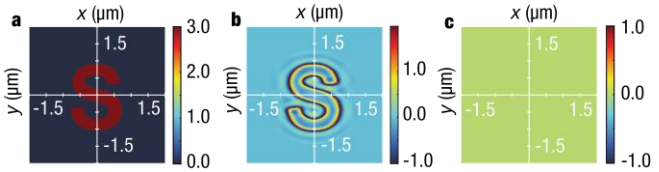

FIG. 8. Invisibility on demand procedure applied with two symmetrically shaped kernels. (a-c) Complex susceptibility profiles of an "S" shaped object modified with two symmetrically shaped invisibility areas. (a) The real part of the initial object and the (b) real and (c) imaginary parts of the modified complex susceptibility. The invisibility areas are located at (k_x, k_y)=(0, ±11.4)μm^{-1} with a standard deviation of 6.0μm^{-1} in both the k_x and k_y directions.

Figure 8 show the complex susceptibility profiles before (Fig. 8(a)) and after (Fig. 8(b, c)) applying the invisibility procedure for the same "S" shaped object as in Fig. 2(a) (in the main article). As can be noted from this figure, the modified object is composed of a purely real dielectric susceptibility. Furthermore, Fig. 9 shows the FDTD results for such a case, where the suppression of the reflections for both symmetrically placed angle ranges (delimited with white dashed lines) can be observed.

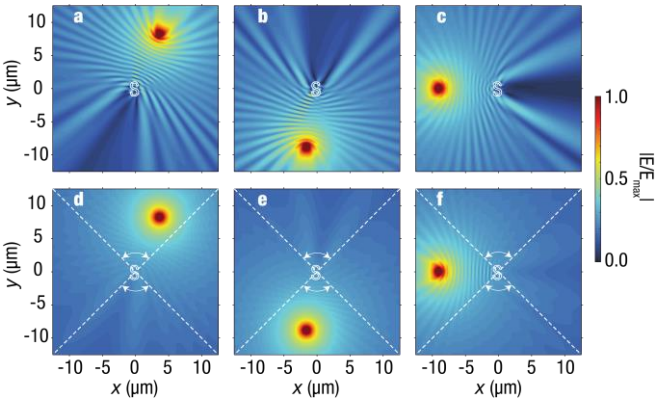

FIG. 9. Reflection test for two symmetrically placed kernels. (a-f) FDTD simulations of waves coming from point sources at different positions for scatterer given in Fig. 8. The upper and lower rows correspond to cases where the invisibility is not-activated and activated, respectively. Excitation angles correspond to (a,d) 24º, (b,e) 190º and (c,f) 270º. The white dashed lines denote the angular range where invisibility is activated. Operational wavelength corresponds to 1.1μm.

[1] J. B. Pendry, D. Schurig, and D. R. Smith, Science. **312**, 1780 (2006).
[2] U. Leonhardt, Science. **312**, 1777 (2006).
[3] J. Li and J. B. Pendry, Phys. Rev. Lett. **101**, 203901 (2008).
[4] L. H. Gabrielli, J. Cardenas, C. B. Poitras, and M. Lipson, Nat. Photonics **3**, 461 (2009).
[5] J. Valentine, J. Li, T. Zentgraf, G. Bartal, and X. Zhang, Nat. Mater. **8**, 568 (2009).
[6] T. Ergin, N. Stenger, P. Brenner, J. B. Pendry, and M. Wegener, Science. **328**, 337 (2010).
[7] M. Gharghi, C. Gladden, T. Zentgraf, Y. Liu, X. Yin, J. Valentine, and X. Zhang, Nano Lett. **11**, 2825 (2011).
[8] A. Alù and N. Engheta, Phys. Rev. E - Stat. Nonlinear, Soft Matter Phys. **72**, 016623 (2005).
[9] D. Rainwater, A. Kerkhoff, K. Melin, J. C. Soric, G. Moreno, and A. Alù, New J. Phys. **14**, (2012).
[10] P. Y. Chen and A. Alù, Phys. Rev. B - Condens. Matter Mater. Phys. **84**, 205110 (2011).
[11] D. Ye, L. Lu, J. D. Joannopoulos, M. Soljačić, and L. Ran, Proc. Natl. Acad. Sci. **113**, 2568 (2016).
[12] Y. Urzhumov, N. Landy, T. Driscoll, D. Basov, and D. R. Smith, Opt. Lett. **38**, 1606 (2013).
[13] H. Chen, C. T. Chan, and P. Sheng, Nat. Mater. **9**, 387 (2010).
[14] R. Fleury and A. Alu, Prog. Electromagn. Res. **147**, 171 (2014).
[15] M. Kulishov, J. M. Laniel, N. Bélanger, J. Azaña, and D. V. Plant, Opt. Express **13**, 3068 (2005).
[16] Z. Lin, H. Ramezani, T. Eichelkraut, T. Kottos, H. Cao, and D. N. Christodoulides, Phys. Rev. Lett. **106**, 213901 (2011).
[17] S. Longhi, J. Phys. A Math. Theor. **44**, (2011).
[18] A. Regensburger, C. Bersch, M. A. Miri, G. Onishchukov, D. N. Christodoulides, and U. Peschel, Nature **488**, 167 (2012).
[19] L. Ge, Y. D. Chong, and A. D. Stone, Phys. Rev. A - At. Mol. Opt. Phys. **85**, 023802 (2012).
[20] L. Feng, Y. L. Xu, W. S. Fegadolli, M. H. Lu, J. E. B. Oliveira, V. R. Almeida, Y. F. Chen, and A. Scherer, Nat. Mater. **12**, 108 (2013).
[21] A. Mostafazadeh, Phys. Rev. A - At. Mol. Opt. Phys. **87**, 012103 (2013).
[22] S. Longhi, Opt. Lett. **40**, 5694 (2015).
[23] S. A. R. Horsley, C. G. King, and T. G. Philbin, J. Opt. **18**, (2016).
[24] S. Longhi, Opt. Lett. **41**, 3727 (2016).
[25] X. F. Zhu, Y. G. Peng, D. G. Zhao, Opt. Express **22**, 18401 (2015).
[26] S. A. R. Horsley, M. Artoni, and G. C. La Rocca, Nat. Photonics **9**, 436 (2015).
[27] FDTD calculations are performed using Lumerical Solutions, Inc. software. http://www.lumerical.com/tcad-products/fdtd/
[28] D. Ye, C. Cao, T. Zhou, J. Huangfu, G. Zheng, and L. Ran, Nat. Commun. **8**, (2017).
[29] W. Jiang, Y. Ma, J. Yuan, G. Yin, W. Wu, and S. He, Laser Photonics Rev. **11**, (2017).
[30] S. A. R. Horsley and S. Longhi, Phys. Rev. A 96, 023841 (2017).
[31] B. Peng, S. K. Özdemir, F. Lei, F. Monifi, M. Gianfreda, G. L. Long, S. Fan, F. Nori, C. M. Bender, and L. Yang, Nat. Phys. **10**, 394 (2014).
[32] M. Lawrence, N. Xu, X. Zhang, L. Cong, J. Han, W. Zhang, and S. Zhang, Phys. Rev. Lett. **113**, 093901 (2014).
[33] L. Feng, M. Ayache, J. Huang, Y. L. Xu, M. H. Lu, Y. F. Chen, Y. Fainman, A. Scherer, and S. M. Sze, Science **333**, 729 (2011).
[34] B. Zhen, C. W. Hsu, Y. Igarashi, L. Lu, I. Kaminer, A. Pick, S. L. Chua, J. D. Joannopoulos, and M. Soljačić, Nature **525**, 354 (2015).